How to cite: *Angew. Chem. Int. Ed.* **2023,** *62,* e202217530
International Edition: doi.org/10.1002/anie.202217530
German Edition: doi.org/10.1002/ange.202217530

Organic Light-Emitting Didoes

TADF Invariant of Host Polarity and Ultralong Fluorescence Lifetimes in a Donor-Acceptor Emitter Featuring a Hybrid Sulfone-Triarylboron Acceptor**

Mateusz Urban, Paulina H. Marek-Urban, Krzysztof Durka, Sergiusz Luliński,* Piotr Pander,* and Andrew P. Monkman*

Abstract: 10*H*-Dibenzo[*b*,*e*][1,4]thiaborinine 5,5-dioxide (**SO2B**)—a high triplet ($T_1 = 3.05$ eV) strongly electron-accepting boracycle was successfully utilised in thermally activated delayed fluorescence (TADF) emitters **PXZ-Dipp-SO2B** and **CZ-Dipp-SO2B**. We demonstrate the near-complete separation of highest occupied and lowest unoccupied molecular orbitals leading to a low oscillator strength of the $S_1 \rightarrow S_0$ CT transition, resulting in very long *ca.* 83 ns and 400 ns prompt fluorescence lifetimes for **CZ-Dipp-SO2B** and **PXZ-Dipp-SO2B**, respectively, but retaining near unity photoluminescence quantum yield. OLEDs using **CZ-Dipp-SO2B** as the luminescent dopant display high external quantum efficiency (EQE) of 23.3 % and maximum luminance of 18600 cd m^{-2} with low efficiency roll off at high brightness. For **CZ-Dipp-SO2B**, reverse intersystem crossing (rISC) is mediated through the vibronic coupling of two charge transfer (CT) states, without involving the triplet local excited state (^{3}LE), resulting in remarkable rISC rate invariance to environmental polarity and polarisability whilst giving high organic light-emitting diode (OLED) efficiency. This new form of rISC allows stable OLED performance to be achieved in different host environments.

Introduction

Organic Light-Emitting Diodes (OLEDs) have been a subject of intensive studies over the past two decades. They are currently widespread in consumer electronics as part of high-end luminescent displays.[1–3] OLEDs are characterized by high luminous efficiency and low energy consumption while displaying features important from the point of potential applications: a broad range of colours, wide viewing angles, sunlight-readability, high contrast, and attractive mechanical properties, such as flexibility.[1,3–5] The physical processes underpinning charge recombination in OLEDs lead to a spin statistical 25:75 ratio between singlet and triplet excitons in the emissive layer.[1,6,7] Since three out of every four excited states created in hole-electron recombination are triplets it is fundamental for device efficiency to use emitters able to effectively generate light from these normally dark states. The most prominent examples of such emitters are phosphorescent Pt^{II} and Ir^{III} metal complexes[8,9] and thermally activated delayed fluorescence (TADF) emitters.[10–13] TADF has been known for over 90 years[14,15] but attracted a noteworthy interest only in the past decade. Emerging interest in the use of TADF in OLEDs was motivated by the works of Adachi[10,16,17] and other researchers[7,18,19] demonstrating performances competitive to those of the more conventional phosphorescent dopants. TADF emitters do not require heavy metals in the structure, and therefore are a low-cost alternative to Pt^{II} and Ir^{III} based phosphorescent complexes.

In a typical design of a TADF luminophore one aims to achieve spatial separation between highest occupied and lowest unoccupied molecular orbitals (HOMO and LUMO), to reduce the electron exchange energy, and thus to minimise the singlet-triplet energy gap (ΔE_{ST}).[7,20,21] Small ΔE_{ST} values, typically < 0.2 eV, allow thermal up-conversion of triplet to singlet states via reverse intersystem crossing (rISC). When the singlet and triplet states involved (most frequently charge transfer states) become effectively degenerate and electron exchange energy becomes negligible, but the spin orbit coupling between them approaches zero and the interconversion, rISC, between them becomes forbidden as orbital angular momentum cannot change during the transition.[22] However, it has been shown both theoretically[23,24] and experimentally,[25–27] that a second energetically close triplet state, such as a local triplet state of

[*] M. Urban, P. H. Marek-Urban, K. Durka, S. Luliński
Faculty of Chemistry, Warsaw University of Technology
Noakowskiego 3, 00-664 Warsaw (Poland)
E-mail: krzysztof.durka@pw.edu.pl
sergiusz.lulinski@pw.edu.pl
P. Pander
Faculty of Chemistry, Silesian University of Technology
Strzody 9, 44-100 Gliwice (Poland)
E-mail: piotr.pander@polsl.pl
M. Urban, P. Pander, A. P. Monkman
Department of Physics, Durham University
South Road, Durham DH1 3LE (UK)

[**] A previous version of this manuscript has been deposited on a preprint server (https://doi.org/10.26434/chemrxiv-2022-hrc86).

donor (D) or acceptor (A), can mediate second order vibronic coupling (SOC), giving rise to fast, allowed ISC and rISC. However, decoupling HOMO and LUMO also reduces the oscillator strength of the $S_1 \rightarrow S_0$ transition, leading to weak or non-luminescent behaviour if non-radiative processes are comparably fast. Recent new strategies have led to an increase of the HOMO–LUMO spatial overlap without detrimentally effecting the ΔE_{ST}, i.e. via using multiple donor/acceptor moieties[28,29] or homoconjugation,[30] often demonstrating increased $S_1 \rightarrow S_0$ transition oscillator strength. However, it remains challenging to develop systems with $\Delta E_{ST} \rightarrow 0$ which maintain highly-efficient luminescence despite a near-forbidden $S_1 \rightarrow S_0$ transition.

The most common way to achieve HOMO–LUMO decoupling is through a charge transfer (CT) excited state. Diaryl sulfones are highly popular among various organic acceptors used as key building blocks in TADF emitters.[16,17,27,31–38] Significant advantage of the sulfonyl group comes from its tetrahedral geometry which reduces π-conjugation leading to a high singlet and triplet excited state energy desirable in blue emitters.[39] Sulfones exhibit very high thermal stability which is advantageous for OLED applications.[40] Similarly, electron-deficient three-coordinate organoboron compounds with an empty 2p orbital on the boron atom are strongly desired as building blocks of acceptors used in TADF emitters. Organoboron TADF emitters have demonstrated high efficiency when used in OLEDs as emitters: up to 100 % internal quantum efficiency (IQE) or 20–30 % external quantum efficiency (EQE) without out-coupling enhancements.[41–43]

Here we present a new acceptor with high triplet energy ($T_1 = 3.05$ eV) which combines the electron deficient character of a boron atom with an electron-withdrawing sulfone group within a central heterocylic ring of dibenzo[*b*,*e*]-[1,4]thiaborinine 5,5-dioxide (**SO2B**). Although there exist examples of triarylboranes constituting electron deficient sulfone,[44] sulfoxide[45] or cationic methylsulfonium[46] groups, our **SO2B** acceptor is functionally and structurally different from them and features the sulfone and triarylborane units in the same heterocycle. The structural design is complemented with conventional donors such as phenoxazine (**PXZ**) and carbazole (**CZ**) separated from the boracyclic moiety by a phenylene π-spacer with two attached bulky isopropyl groups (**Dipp**). The molecules are found to have near-zero ΔE_{ST} and simultaneously display extremely long-lived emissive singlet charge transfer (^{1}CT) states, indicative of a very high degree of HOMO–LUMO electronic decoupling. We demonstrate that this is due to the strongly electron-acceptor property of the **SO2B** unit and the spatially locked **Dipp** spacer. This configuration also effectively prevents non-radiative decay, yielding high photoluminescence quantum yield, and excellent TADF performance. Our new strategy overcomes the usual trade-off between small ΔE_{ST} and fast radiative decay from the S_1 state, hence yielding high photoluminescence quantum yield (PLQY, Φ_{PL}) in TADF systems.[30] But, at the same time whilst still using the conventional donor-π-spacer-acceptor (D-π-A) design,[47] and we also achieve host environment stability never before reported, because of the states involved in rISC.

Results and Discussion

The synthesis of 10-hydroxy-10*H*-dibenzo[*b*,*e*]-[1,4]thiaborinine 5,5-dioxide **3** started from di(2-bromophenyl)sulfoxide **1**, which was obtained from 1,2-dibromobenzene (Figure 1a).[48] The resultant sulfoxide was oxidized to sulfone **2** which was further subjected to double Br-Li exchange followed by transmetallation with $Cl_2BN(i\text{-}Pr)_2$, giving rise to heterocyclic borinic acid **3** isolated as a white solid after aqueous workup. Compound **3** is stable under ambient conditions. X-ray diffraction indicates that molecular structure of **3** strongly deviates from planarity (Figure 1b).[49] The ^{11}B NMR analysis shows that **3** coordinates solvent molecule in DMSO-d_6 solution {$\delta(^{11}B) = 6.5$ ppm}. As a next step **3** was converted to a 10-chloro derivative **4**. According to single crystal X-ray diffraction analysis, **4** exists as a centrosymmetric dimer through formation of S=O→B dative bonds (Figure 1c).[49] ^{1}H NMR analysis indicates that the dimeric structure is preserved in

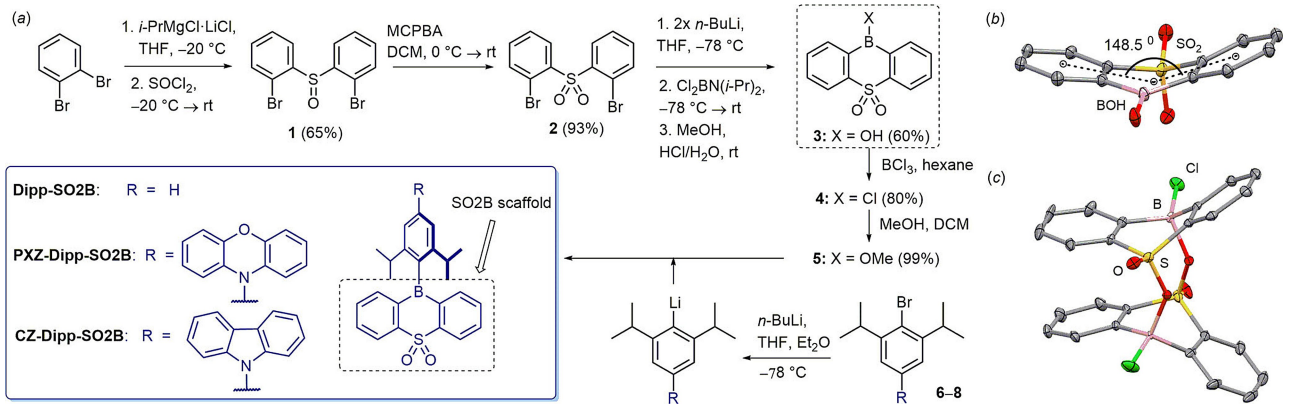

Figure 1. (a) Synthesis of **Dipp-SO2B**, **PXZ-Dipp-SO2B** and **CZ-Dipp-SO2B**. Molecular structures of (b) **3** and (c) **4** determined by single-crystal X-ray diffraction (ellipsoids drawn at the 50% probability level, H-atoms are omitted for clarity).

$CDCl_3$ and C_6D_6 solutions whilst in the presence of Et_2O or THF it equilibrates with monomeric form with solvent molecule coordinated to the boron centre (Figures S9.12–9.18 in the Supporting Information). The reactivity of such species proved to be strongly limited due to tetrahedral environment around the boron atom. Thus, **4** was converted to a 10-methoxy derivative **5**. Our attempts to directly converting **2** or **3** into **5** have not been successful (details in the Supporting Information, Section 8). Theoretical calculations suggest that the monomeric form of **5** should be preferred in solution although ^{1}H, ^{11}B and ^{13}C NMR spectroscopy data point at a likely equilibrium between dimeric and monomeric forms in $CDCl_3$ and THF-d_8 solutions. Nevertheless, the monomeric form dominates in solution which results in a higher reactivity of **5** towards nucleophiles than that of **4**, despite lower Lewis acidity of the former. Final compounds **Dipp-SO2B**, **PXZ-Dipp-SO2B** and **CZ-Dipp-SO2B** were obtained from **5** and aryl bromides **6**–**8** after Br-Li exchange with *n*-BuLi. Obtained products show good chemical stability and are stable under ambient conditions. They also exhibit high thermal stability from the standpoint of OLED fabrication. Thermogravimetric analysis (TGA) revealed that their decomposition temperatures T_d (corresponding to 5 % weight loss) are 280 and 300 °C for **PXZ-Dipp-SO2B** and **CZ-Dipp-SO2B**, respectively (Figures S5.2 and S5.3, Supporting Information). The ^{1}H NMR spectra recorded before and after irradiation with a 365 nm, 26 W LED strip light for 1 h (Figures S5.4 and S5.5, Supporting Information) are identical indicating high photostability. The crystal structures of **PXZ-Dipp-SO2B** and **CZ-Dipp-SO2B** were determined by X-ray diffraction (Figure 2).[49] We find that the phenylene spacer is near orthogonal to the mean plane of the boracyclic acceptor (**SO2B**) fragment in both of the presented structures. The crystallographic data point to a highly restricted mutual rotation between the **SO2B** and **Dipp** units and some degree of conformational freedom in other parts of the molecules. The ^{1}H diffusion-ordered spectroscopy nuclear magnetic resonance (DOSY ^{1}H NMR) analysis performed for **CZ-Dipp-SO2B** indicates that it exists as the monomer in $CDCl_3$ solution, in contrast with varying tendency to aggregation observed for precursors. This results from the steric hindrance at the boron atom provided by two isopropyl groups.

We used density functional theory (DFT) and time-dependant density functional theory (TD-DFT) calculations performed at the B3LYP/6-311++G(d,p) level of theory to support the experimental findings. Our calculations confirmed a very strong electron-accepting capability of the **SO2B** core with its LUMO energy slightly below −3.0 eV. This ranks **SO2B** among one of the strongest organoboron acceptors currently known to be used in TADF lumino-

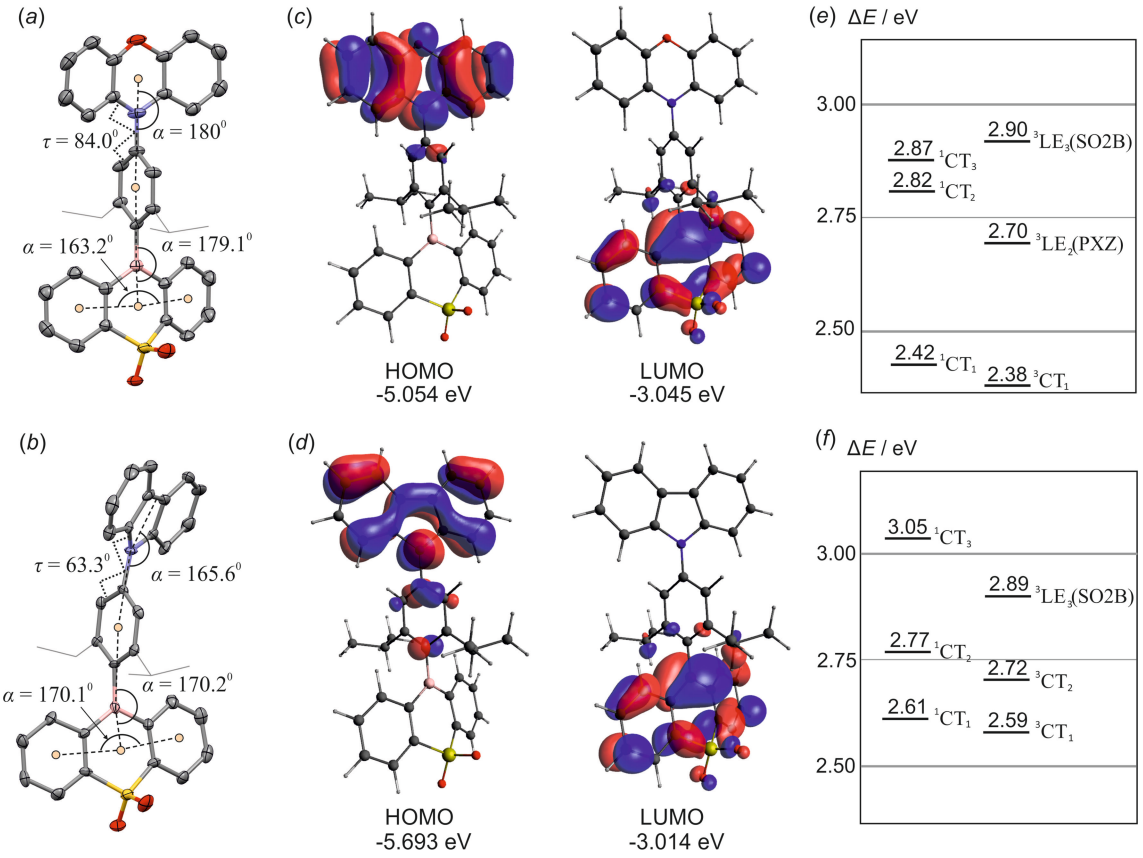

Figure 2. Molecular structures of (a) **PXZ-Dipp-SO2B** and (b) **CZ-Dipp-SO2B** determined from single-crystal X-ray diffraction (ellipsoids drawn at the 50% probability level, H-atoms are omitted for clarity).[49] (c, d) Frontier molecular orbital contours. Excited state energy diagrams for (e) **PXZ-Dipp-SO2B** and (f) **CZ-Dipp-SO2B**.

phores (Figure S6.1 in the Supporting Information). This is also reflected in the experimental LUMO energy of *ca.* −3.5 eV obtained from cyclic voltammetry. At this point we note that the **SO2B** acceptor is so strong that it forms a CT state even with the very weak Dipp donor. A similar phenomenon has been observed previously with another very strong organoboron acceptor: 9,10-dimesityl-9,10-dihydro-9,10-diboraanthracene.[50,51] In **PXZ-Dipp-SO2B** and **CZ-Dipp-SO2B**, separation of HOMO and LUMO between the donor and acceptor units (Figure 2) clearly points at a strong CT character of the resultant excited state. This, in turn, results in a very small ^{1}CT-^{3}CT ΔE_{ST} for **PXZ-Dipp-SO2B** and **CZ-Dipp-SO2B**, below 0.1 eV, respectively. A larger ΔE_{ST} value is found for **Dipp-SO2B**, at about 0.34 eV (Figure S6.4 and Table S6.1 in the Supporting Information).

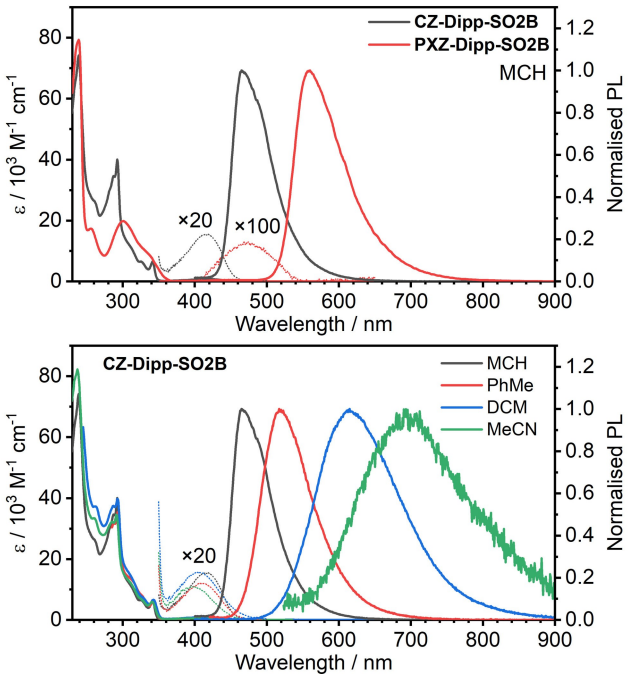

Figure 3. Steady state absorption and photoluminescence spectra: (top) **CZ-Dipp-SO2B** and **PXZ-Dipp-SO2B** in dilute MCH solution; (bottom) **CZ-Dipp-SO2B** in solvents of various polarity indicated in figure legend. Note that for photoluminescence spectrum of **CZ-Dipp-SO2B** in MeCN only the CT band is shown. λ_{exc} = 355 nm.

We have investigated the photoluminescent behaviour of **Dipp-SO2B**, **CZ-Dipp-SO2B** and **PXZ-Dipp-SO2B** to give an insight into their delayed fluorescence characteristics and the mechanisms underpinning their observed luminescence behaviour. Key photophysical characteristics are presented in Figures 3 and 6 and Table 1, while supplementary data are presented in the Supporting Information, Figures S3.1–S3.12. First, we note that all three molecules show a pronounced positive fluorescence solvatochromism, whilst small solvatochromic shifts are also observable in the weak ($\varepsilon < 1000\ M^{-1}cm^{-1}$) long wavelength absorption bands in each case (see Figure 3 and Figure S3.3 in the Supporting Information). These charge-transfer bands display a positive solvatochromic shift of their onsets, but a clear negative shift of band maxima—a phenomenon worthy of a further investigation in the future. **CZ-Dipp-SO2B** shows the most striking solvatochromic shift (230 nm or 7120 cm^{-1}), comparable to if not larger than that of the strongest solvatochromic dyes.[52–55] This we believe arises through both near perfect orthogonality of D and A plus the increased spatial separation of the electron and hole across the phenyl ring spacer unit, yielding near perfect complete one electron transfer in the CT state. Its photoluminescence colour varies from blue in methylcyclohexane (MCH), λ_{em} = 465 nm, through green in toluene, λ_{em} = 520 nm, to red in dichloromethane (DCM), λ_{em} = 615 nm, with a further shift towards near infrared (NIR) in acetonitrile (MeCN), λ_{em} = 695 nm (see Figure 3 *bottom*). The above findings demonstrate a strong CT character to the S_1 state in all three molecules and suggest a very small oscillator strength of the $S_0 \rightarrow S_1$ transition, in agreement with calculations. Properties of CT emitters recorded in low polarity solvents and matrices are often more relevant for OLEDs, therefore we decide to

Table 1: Key photophysical characteristics of **PXZ-Dipp-SO2B** and **CZ-Dipp-SO2B** at RT.

	Solvent/matrix	λ_{abs}/nm [$\varepsilon/10^3$ $M^{-1}cm^{-1}$][a]	λ_{em}/nm[b]	Φ_{PL}[c]	Φ_{DF}/Φ_{PF}[d]	τ_{PF}/ns[e]	τ_{TADF}/μs[f]	k_r^S/ 10^6 s^{-1}[g]	k_{rISC}/ 10^4 s^{-1}[h]
CZ-Dipp-SO2B	MCH	417 [0.8], 342 [6], 293 [37], 238 [74]	465	1.00	0.26	83	4.0	9.6	6.5
	Zeonex	–	474	1.00	0.28	82 (68%); 27 (32%) τ_{av} = 75[i]	3.8 (98%); 8.1 (2%) τ_{av} = 4.0[i]	10[j]	6.9[j]
PXZ-Dipp-SO2B	MCH	475 [0.1], 338sh [8], 300 [20], 258 [17], 240 [80]	560	0.75	0.14	394	5.6	1.7	1.8
	Zeonex	–	575	0.93	0.15	223 (62%); 636 (38%) τ_{av} = 486[i]	12.5	1.7[j]	1.1

[a] UV/Vis absorption maxima and extinction coefficients, sh = shoulder; [b] steady state PL maxima; [c] Total photoluminescence quantum yield (Φ_{PL}) in degassed solution or under N_2 in film; [d] Ratio of photoluminescence quantum yield of delayed fluorescence (Φ_{DF}) to prompt fluorescence (Φ_{PF}); [e] Radiative decay lifetime of prompt fluorescence; [f] Radiative decay lifetime of TADF; [g] Radiative decay rate of the S_1 state, $k_r^S = \Phi_{PF}/\tau_{PF}$; [h] Obtained as previously reported.[30] All values determined at room temperature; [i] Average lifetime $\tau_{av} = (A_1\tau_1^2 + A_2\tau_2^2)/(A_1\tau_1 + A_2\tau_2)$; [j] Based on average lifetime values.

focus our studies on MCH solutions and Zeonex films.[56,57] **Dipp-SO2B** due to its large ΔE_{ST} does not give DF at room temperature, therefore, in this work we focus on the other two compounds. We note that **CZ-Dipp-SO2B** and **PXZ-Dipp-SO2B** demonstrate unusually long-lived prompt fluorescence decay lifetimes in MCH, $\tau_{PF}=83$ ns and $\tau_{PF}=$ 394 ns, respectively. We record a high $\Phi_{PL}=1.0$ and 0.75 in MCH solution and $\Phi_{PL}=1.0$ and 0.93 in Zeonex films, respectively for **CZ-Dipp-SO2B** and **PXZ-Dipp-SO2B**. These long fluorescence lifetimes correspond to $S_1\rightarrow S_0$ radiative rates k_r^S $9.6\times10^6\,s^{-1}$ and $1.7\times10^6\,s^{-1}$, respectively for **CZ-Dipp-SO2B** and **PXZ-Dipp-SO2B**. As the $\Phi_{PL}\approx1$, we can calculate the ratio of prompt to delayed fluorescence contributions from the area under each decay component (Table 1). In MCH this gives prompt emission yields of 0.79 and 0.66 respectively for **CZ-Dipp-SO2B** and **PXZ-Dipp-SO2B**.

In order to correlate the long photoluminescence lifetimes with the properties of the $S_0\rightarrow S_1$ transition, we estimated the k_r^S values from steady state absorption and fluorescence spectra using the Strickler and Berg method.[58] The estimates, $6.6\times10^6\,s^{-1}$ (oscillator strength $f=0.015$) and $1.4\times10^6\,s^{-1}$ ($f=0.004$), respectively for **CZ-Dipp-SO2B** and **PXZ-Dipp-SO2B**, are in excellent agreement with experiment, confirming that the observed long-lived emission is consistent with prompt fluorescence from the S_1. These findings identify three fundamental conditions that are met simultaneously in these new emitters to explain the observed luminescent behaviour: (**1**) oscillator strength of the $S_1\rightarrow S_0$ transition is very low, indicative of highly decoupled HOMO and LUMO, giving very long radiative lifetimes; (**2**) highly restricted molecular motion of the **Dipp-SO2B** moiety resulting from the steric effect of the two isopropyl groups in the Dipp linker is contributing to very slow rates of non-radiative decay, ensuring high PLQY; (**3**) intersystem crossing rates to T_1 are extremely low, resulting in a small triplet formation yield (under optical excitation) again ensuring high prompt PLQY- this aspect will be discussed later in more detail. The structural conditions required for these properties have been confirmed with computational and X-ray diffraction studies discussed above. Previous accounts of a similar long prompt fluorescence behaviour have been demonstrated independently in different CT TADF systems with reports of ≈100 ns[59] and ≈400 ns[60] decay lifetimes, the former in a structurally-related emitter with a boron-based acceptor and Dipp π-linker. We will discuss these accounts together with delayed fluorescent properties of **CZ-Dipp-SO2B** and **PXZ-Dipp-SO2B**.

Another repercussion of the very small electron exchange energy in these new materials is the near forbidden nature of ISC, as first pointed out by Lim et al.[22] Hence, in the optical measurements the rate of triplet production will be very slow and result in low triplet populations. To achieve any meaningful ISC rate the ISC mechanism itself needs to be enhanced by vibronic coupling. This is more likely in **CZ-Dipp-SO2B** were the first two singlet states are some 160 meV apart, whereas in **PXZ-Dipp-SO2B** they are more than 400 meV apart.

As well as these unusual findings presented above, **CZ-Dipp-SO2B** and **PXZ-Dipp-SO2B** display a typical behaviour of strong TADF luminophores. We observe a weak, short-lived blue emission from upper-lying singlet states that is usual for molecules with strongly electronically decoupled HOMO and LUMO.[61,62] We hypothesise the state decays in competition with (relatively) slow electron transfer because of the highly decoupled D and A (Figures 4 and 5).[61] From the time-resolved decay spectra, Figure 4, we see that the energy of the fast decay feature is dependent on the donor, hence we assume it is emission from an initially excited D unit in each case. TADF lifetimes recorded in MCH are 4.0 μs and 5.6 μs, for **CZ-Dipp-SO2B** and **PXZ-Dipp-SO2B**, respectively.

We used Zeonex films for temperature-dependent measurements where it is easier to study photophysical properties in a broad (80–300 K) range of temperatures (Figure 5). The behaviour in Zeonex is in general identical to that in MCH at room temperature, with prompt and delayed fluorescence lifetimes and overall decay traces being similar (Table 1, Figure 6 *top*). We identified the TADF component based on its typical temperature-dependent behaviour (Figure 6 *bottom*) and linear dependence of luminescence intensity on excitation dose (Figure S3.7).[63] Contrary to what would normally be expected with a stronger donor, **PXZ-Dipp-SO2B** displays a longer TADF lifetime than **CZ-Dipp-SO2B** both in Zeonex and MCH. This phenomenon can be

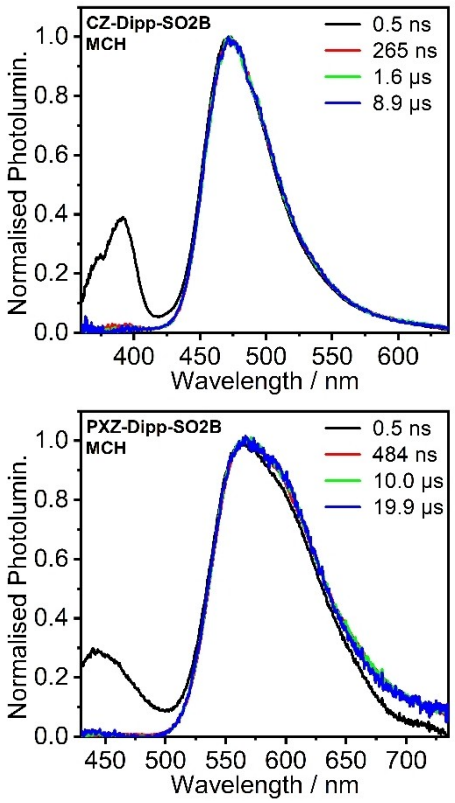

Figure 4. Time-resolved photoluminescence spectra of **CZ-Dipp-SO2B** and **PXZ-Dipp-SO2B** in degassed dilute MCH solutions at RT. $\lambda_{exc}=355$ nm.

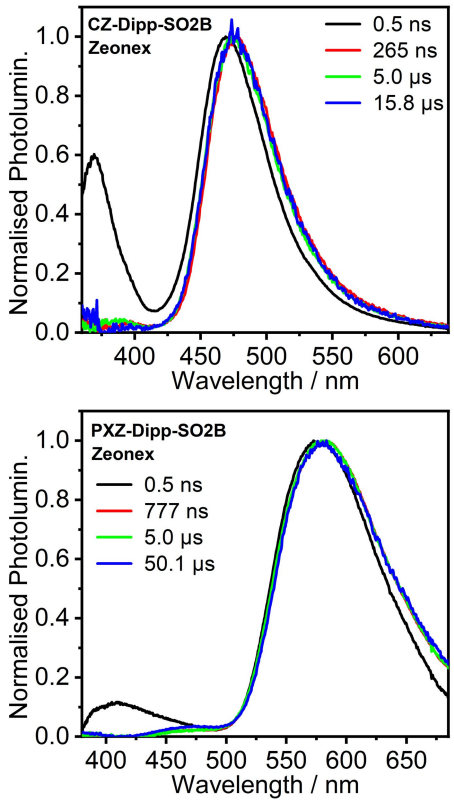

Figure 5. Time-resolved photoluminescence spectra of **CZ-Dipp-SO2B** and **PXZ-Dipp-SO2B** in dilute Zeonex films at RT. $\lambda_{exc} = 355$ nm.

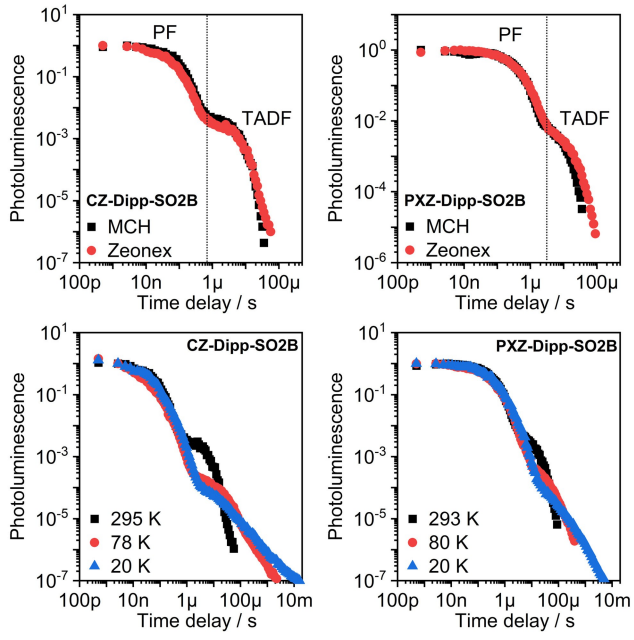

Figure 6. (top) Photoluminescence decay traces in dilute MCH solutions and Zeonex films at room temperature. A thin dotted line indicates the separation between prompt (PF) and delayed (TADF) fluorescence exponential regimes. (bottom) Photoluminescence decay traces in dilute Zeonex films at temperatures indicated in figure legend. $\lambda_{exc} = 355$ nm.

explained by the smaller k_r^S and slower ISC/rISC due to less favourable SOC pathways in **PXZ-Dipp-SO2B**.[24,64,65] Moreover, **PXZ-Dipp-SO2B** in Zeonex displays a third, weak long-lived component on the timescale extending beyond 100 µs at room temperature (Figure S3.1). We note that this component is too weak to be resolved in the decay traces. This new component, also present at lower temperatures, displays characteristics typical of phosphorescence from a local excited triplet state of the acceptor (^3LE_A) moiety.

Temperature-dependent photoluminescence decays measured in dilute Zeonex films (Figure 6 *bottom*) reveal a typical picture of TADF emitters with the delayed fluorescence decay time increasing as the temperature decreases. We observed that delayed fluorescence persists even at 80 K and the phosphorescence spectrum cannot be identified with confidence, a feature in common with other TADF systems showing extremely narrow ΔE_{ST}.[66,67] For **CZ-Dipp-SO2B** we observed no change in emission onset at room temperature, 80 K or 20 K between 500 ns and 2 ms delay (Figure S3.6). Furthermore, no obvious local phosphorescence emission is observed for **CZ-Dipp-SO2B**. This is though completely in-line with our calculations that show the two lowest energy triplet states are of CT character, and the lowest local triplet state is 300 meV above the lowest CT triplet state (Figure 2). Thus, we would not expect to observe any local character phosphorescence. From these observations it is clear that in the case of **CZ-Dipp-SO2B** the second order vibronic coupling SOC cannot be efficiently mediated by the lowest energy ^{3}LE triplet state, energetically it is too far away from the ^{3}CT states to give a high rISC rate. However, the second lowest triplet state, $^3CT_2$, also a CT state but very close in energy to $^3CT_1$, is ca. 130 meV above so that the $^3CT_2$ acts as the mediator in this case. Calculations show (see Figure 2, Figure S6.8 and Table S6.1 in Supporting Information) that $^3CT_2$ has a different orbital character to $^3CT_1$ allowing efficient SOC to $^1CT_1$, thus the SOC matrix element $<^1CT_1|H_{SO}|^3CT_2> \neq 0$. In this case, as polarity increases, all the CT states relax by about the same energy, such that the relative energy gaps between each state do not change. rISC rate in this case is then effectively independent of environment, an extremely important new property for stable device application. The ^{1}CT state in our molecules has a very long radiative lifetime, but $\Phi_{PL} \approx 1$, implying negligible non-radiative decay from internal conversion. Thus, with the degenerate ^{3}CT state being the lowest energy triplet state then it also must have negligible non-radiative decay. Therefore, the lowest triplet state ^{3}CT will be very effectively decoupled from the singlet ground state allowing these states to be efficient reservoirs of triplet states with little non-radiative lose.[68] Whereas, for **PXZ-Dipp-SO2B**, $^3CT_2$ is energetically significantly above $^3CT_1$ such that $^3LE_1$ is below it and should be the mediator state. In this case we expect a slow rISC due to the large $^3LE_1$-$^3CT_1$ energy gap of 320 meV. As polarity increases the $^1CT_1$-$^3CT_1$ relax and move even further away from the $^3LE_1$ leading to significantly lower rISC efficiency. The effect of this behaviour directly affects device performance as we demonstrate below.

Returning to the subject of long prompt fluorescence lifetimes in **CZ-Dipp-SO2B** and **PXZ-Dipp-SO2B** and their vital importance for description of TADF systems. In earlier accounts of long-lived ($\tau \approx 100$–400 ns) mono-exponential radiative decay originating from CT states,[59,60] the authors have not observed any additional longer-lived components typical for metal-free TADF compounds ($\tau \approx 1$–10 µs) and assigned the submicrosecond decay component to TADF. Such mono-exponential TADF decay without any prompt fluorescence component is typical for heavy-metal complexes where the spin-orbit coupling between singlet and triplet states induced by the metal leads to extremely fast intersystem crossing (ISC) rates.[65,69,70] Such a fast ISC is unlikely to occur in compounds without heavy atoms. Interestingly, another recent work also reports long prompt fluorescence lifetimes ($\tau \approx 100$ ns) in diboron-based yellow-orange emitters where a weak, but well-resolved TADF component is observed.[59] Our results strongly suggest that very long-lived prompt fluorescence, as in **CZ-Dipp-SO2B** and **PXZ-Dipp-SO2B** or in the reported cases highlighted, must involve slow intersystem crossing which result in relatively low population of triplet states with optical excitation. In **CZ-Dipp-SO2B** and **PXZ-Dipp-SO2B** this leads to only modest contributions of TADF to the overall emission, 21–22 % and 12–13 %, respectively. Potentially, even smaller contributions of TADF can characterise other systems which hinders detection of the TADF component with optical excitation. Luminescence quenching by oxygen is often incorrectly used as evidence for a triplet origin of this emission. We demonstrate (Figure S3.13, Supporting Information) that such experiments are not specific enough, and long-lived prompt fluorescence ($S_0 \rightarrow S_1$) is subject to similar quenching, in line with our previous reports.[71]

To demonstrate TADF performance of **PXZ-Dipp-SO2B** and **CZ-Dipp-SO2B** we have used them as emissive dopants in proof-of-concept highly efficient vacuum-deposited (Figure 7, Tables S7.1 and S7.2 in the Supporting Information) and solution-processed (Tables S7.3, Figures S7.1-S7.6 in the Supporting Information) OLEDs. Devices had the general structure; dipyrazino[2,3-*f*:2′,3′-*h*]quinoxaline-2,3,6,7,10,11-hexacarbonitrile (HAT-CN) hole injection layer and 4,4′-(diphenylsilanediyl)bis(*N*,*N*-diphenylaniline) (TSBPA) hole transport, electron blocking layer. 1,3,5-tris[(3-pyridyl)-phen-3-yl]benzene (TmPyPB) or 2,4,6-tris[3-(diphenylphosphinyl)phenyl]-1,3,5-triazine (PO-T2T) served as electron transport and hole blocking layers, with a LiF/Al electron injection layer. Initially, a device structure using 1,3-bis(carbazol-9-yl)benzene (mCP) host and TmPyPB electron transport material was employed, but gave modest luminance and an elevated turn-on voltage (V_{ON}). An optimised blend host comprising mCP (HOMO −5.9 eV) or 4,4′,4-tris(carbazol-9-yl)triphenylamine (TCTA) (HOMO −5.7 eV) and PO-T2T (LUMO −3.1 eV) was used as their energy levels[67] match those of **CZ-Dipp-SO2B** (HOMO −5.89 eV, LUMO −3.46 eV) and **PXZ-Dipp-SO2B** (HOMO −5.32 eV, LUMO −3.51 eV), respectively. In this case a structure ITO | HAT-CN (10 nm) | TSBPA (40 nm) | mCP (2 nm) | mCP:PO-T2T (80:20) co 5 % **CZ-Dipp-SO2B** (20 nm) | PO-T2T (50 nm) | LiF (0.8 nm) | Al (100 nm) was used (Dev1) and ITO | HAT-CN (10 nm) | TSBPA (40 nm) | TCTA (2 nm) | TCTA:PO-T2T (80:20) co 5 % **PXZ-Dipp-SO2B** (20 nm) | PO-T2T (50 nm) | LiF (0.8 nm) | Al (100 nm) (Dev 2). An additional 2 nm mCP or TCTA layer serves as an exciton blocking layer to prevent formation of exciplex states between PO-T2T and TSBPA.[67] This approach led to significantly reducing V_{ON} and increased current density and luminance. Devices of type Dev1 achieved a high EQE of 23.3 %, near the theoretical limit, and a maximum luminance of 18600 cd m^{-2} with $\lambda_{EL} = 515$ nm green-blue electroluminescence, amply demonstrating the effectiveness of **CZ-Dipp-SO2B** as the TADF emitter. By studying 16 pixels from 4 independent OLEDs of structure Dev1, we recorded EQE in the range from 18.1 % to 24.6 % (Figure S7.7 in Supporting Information). The device data presented here therefore displays performance representative of the whole characterised set of devices. The EQE also remains above 20 % until 1000 cd m^{-2} which is excellent for practical applications. For **PXZ-Dipp-SO2B** Dev2 structure gave bright (5200 cd m^{-2}) orange-red electroluminescence at $\lambda_{EL} = 609$ nm and maximum EQE of 6.8 %.

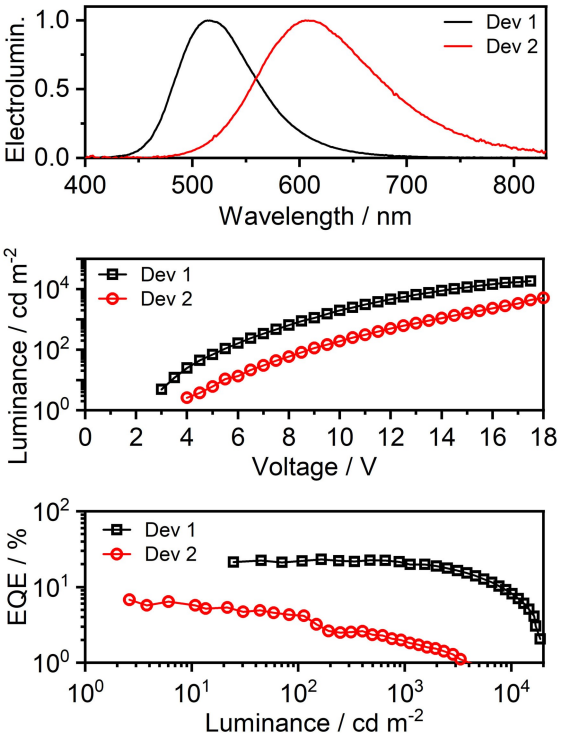

Figure 7. Characteristics of OLED devices 1 and 2: (top) electroluminescence spectra; (middle) luminance vs. voltage; (bottom) external quantum efficiency (EQE) vs. luminance.

From the EL spectra of **CZ-Dipp-SO2B** and **PXZ-Dipp-SO2B** in their respective emissive layers, both materials experience a substantial red shift due to the polarizability of the host. The energy of the CT states shifts by more than 200 meV in respect to MCH or Zeonex. Such a large energy relaxation should greatly affect rISC rate as the ^{3}CT-^{3}LE

energy gap increases by a similar 200 meV. However, in the case of **CZ-Dipp-SO2B** the rISC rate is not affected. As a result near 100 % IQE can be observed even with such a large shift in energy between CT and local triplet states. To demonstrate the host-invariant properties of **CZ-Dipp-SO2B**, OLEDs were produced with a device using bis{4-(*N*-carbazolyl)phenyl}phenylphosphine oxide (BCPO) having a highly polar P=O group mixed with PO-T2T (BCPO:PO-T2T) as host. The new OLEDs, Dev BCPO with structure ITO | HAT-CN (10 nm) | TSBPA (40 nm) | BCPO (2 nm) | BCPO:PO-T2T (85:15) co **CZ-Dipp-SO2B** (5 %) (20 nm) | PO-T2T (50 nm) | LiF (0.8 nm) | Al (100 nm), display comparable EQE of 22.9 %, maximum luminance 20700 cd m^{-2}, and overall similar characteristics to that of the Dev1 devices using mCP:PO-T2T as host (Figures S7.8 and S7.9 in Supporting Information). As described above, **CZ-Dipp-SO2B** introduces a new class of a TADF emitter where clearly all states involved in rISC are CT in character and so all shift by about the same energy with environment. As a result, rISC is unaffected by the strong relaxation of the CT states in the device host. Whereas, for **PXZ-Dipp-SO2B** this is not the case, here $^3LE_1$ acts as the mediator state and therefore the large energetic relaxation of the CT states in the EML greatly increases the energy gap between $^3CT_1$ and $^3LE_1$, significantly reducing the rISC rate. It contributes to the low IQE of **PXZ-Dipp-SO2B** devices. **CZ-Dipp-SO2B** devices also have excellent roll-off performance, somewhat unexpected given the rather modest rISC rates calculated from the optical measurements, Table 1. However, the measured rISC rate may well be limited in the optical measurements through the very slow ISC rate, which is not the case in the devices, and rISC could well be much faster in devices than measured optically, also facilitating excellent roll-off performance. These observations show for the first time a TADF emitter that operates at very close to 100 % IQE and is practically unaffected by host environment over the typical range of host polarisability values, offering much better colour and performance stability, invariant of small batch to batch changes of mixed EML host ratios and also within limits invariant to changes in host material. This can greatly relax fabrication tolerances for devices and increase production yields.

Conclusion

We have developed synthesis of a novel strongly electron-accepting organoboron scaffold **SO2B**. The presence of the sulfone moiety within the boracyclic unit resulted in a significant decrease of LUMO energy compared to related systems. The new **SO2B** acceptor presented in this work features high triplet energy $T_1 = 3.05$ eV and a low-lying LUMO (≈ -3.5 eV), a combination rare among materials used in OLED applications. **SO2B** serves as a key structural component of two new TADF emitters **PXZ-Dipp-SO2B** and **CZ-Dipp-SO2B** featuring a D-π-A architecture and unusually long ($\tau = 83$–394 ns) prompt fluorescence lifetimes. These long fluorescence lifetimes result from suppressing the non-radiative decay by restricting the relative motion of the **SO2B** and **Dipp** units with the bulky isopropyl groups in the latter. We have demonstrated that these long prompt components may lead to reduced triplet formation yield (via optical excitation), thus low intensity of resultant TADF, hindering detection of the delayed fluorescence component in the decay. **CZ-Dipp-SO2B** and especially **PXZ-Dipp-SO2B** with the longer prompt lifetime $\tau = 394$ ns and simultaneously large $\Phi_{PL} = 0.75$ demonstrate that the use of the **SO2B** acceptor and a locked Dipp π-linker provides perfect suppression of non-radiative decay from the singlet state. Our design based on the common D-π-A template overcomes the trade-off between minimising the HOMO–LUMO overlap and reduction in the oscillator strength of the $S_1 \rightarrow S_0$ transition when designing emitters with $\Delta E_{ST} \approx 0$. OLED devices produced using **CZ-Dipp-SO2B** as the emissive dopants have demonstrated excellent TADF performance. The best OLED featuring **CZ-Dipp-SO2B** achieves maximum EQE of 24.6 % and luminance of 17100 cd m^{-2} with $\lambda_{EL} = 515$ nm and excellent roll-off performance. Most importantly, we demonstrate that with **CZ-Dipp-SO2B** the two triplet states that mediate rISC by the second order vibronic coupling spin orbit coupling mechanism are both of CT character. This is different from a more typical ^{3}CT state coupling with a ^{3}LE state. With such a configuration of excited states involving two CT states rather than a CT and an LE state for rISC, the state spacing remains invariant with the polarity or polarizability of the host environment, thus the effectiveness of rISC is not affected by these environmental factors. This then makes production of highly reproducible TADF OLEDs a reality and will allow improvements to host materials to be implemented without having to change the TADF emitter as well to achieve optimum performance. **CZ-Dipp-SO2B** thus introduces a major step forward for the simple utilisation of TADF emitters in OLEDs.

Acknowledgements

The research was funded by Materials_Technologies-3 project granted by Warsaw University of Technology under the programme Excellence Initiative: Research University (ID-UB). P.H.M-U. acknowledges Operational Project Knowledge Education Development 2014–2020 co-financed by the European Social Fund. M.U acknowledges The Iwanowska Programme funded by the Polish National Agency For Academic Exchange (NAWA). APM thanks the EPSRC for funding (EP/T02240X/1). The authors thank Wroclaw Centre for Networking and Supercomputing (http://www.wcss.pl), grant No. 285, for providing computer facilities (*Gaussian16*). Authors also thank Prof. K. Woźniak (University of Warsaw) for providing access to the single-crystal X-ray diffractometer, Dr. Ewa Kaczorowska (Warsaw University of Technology) for performing DOSY ^{1}H NMR experiments and Dr. Marcin Wilczek (University of Warsaw) for performing VT ^{11}B NMR experiments.

Conflict of Interest

The authors declare no conflict of interest.

Data Availability Statement

The data that support the findings of this study are available in the supplementary material of this article.

Keywords: Acceptor · Emitter · Organic Light-Emitting Diodes · Thermally Activated Delayed Fluorescence · Vibronic Coupling

[1] M. Vasilopoulou, A. Fakharuddin, F. P. García de Arquer, D. G. Georgiadou, H. Kim, A. R. bin Mohd Yusoff, F. Gao, M. K. Nazeeruddin, H. J. Bolink, E. H. Sargent, *Nat. Photonics* **2021**, *15*, 656–669.

[2] "New OLED gadget: Oppo F21 Pro/F21 Pro 5G," can be found under https://www.oled-info.com/oppo-f21-pro-f21-pro-5g, **2022**.

[3] K. T. Kamtekar, A. P. Monkman, M. R. Bryce, *Adv. Mater.* **2010**, *22*, 572–582.

[4] J. Fahlteich, C. Steiner, M. Top, D. Wynands, T. Wanski, S. Mogck, E. Kucukpinar, S. Amberg-Schwab, C. Boeffel, N. Schiller, *SID Symp. Dig. Tech. Pap.* **2015**, *46*, 106–110.

[5] R.-P. Xu, Y.-Q. Li, J.-X. Tang, *J. Mater. Chem. C* **2016**, *4*, 9116–9142.

[6] H. Yersin, *Highly Efficient OLEDs with Phosphorescent Materials*, Wiley, Hoboken, **2008**.

[7] Y. Tao, K. Yuan, T. Chen, P. Xu, H. Li, R. Chen, C. Zheng, L. Zhang, W. Huang, *Adv. Mater.* **2014**, *26*, 7931–7958.

[8] Y.-C. Wei, S. F. Wang, Y. Hu, L.-S. Liao, D.-G. Chen, K.-H. Chang, C.-W. Wang, S.-H. Liu, W.-H. Chan, J.-L. Liao, W.-Y. Hung, T.-H. Wang, P.-T. Chen, H.-F. Hsu, Y. Chi, P.-T. Chou, *Nat. Photonics* **2020**, *14*, 570–577.

[9] B. Minaev, G. Baryshnikov, H. Agren, *Phys. Chem. Chem. Phys.* **2014**, *16*, 1719–1758.

[10] H. Uoyama, K. Goushi, K. Shizu, H. Nomura, C. Adachi, *Nature* **2012**, *492*, 234–238.

[11] Y. J. Cho, K. S. Yook, J. Y. Lee, *Adv. Mater.* **2014**, *26*, 4050–4055.

[12] B. S. Kim, J. Y. Lee, *Adv. Funct. Mater.* **2014**, *24*, 3970–3977.

[13] W. Zeng, H.-Y. Lai, W.-K. Lee, M. Jiao, Y.-J. Shiu, C. Zhong, S. Gong, T. Zhou, G. Xie, M. Sarma, K.-T. Wong, C.-C. Wu, C. Yang, *Adv. Mater.* **2018**, *30*, 1704961.

[14] G. N. Lewis, D. Lipkin, T. T. Magel, *J. Am. Chem. Soc.* **1941**, *63*, 3005–3018.

[15] C. A. Parker, C. G. Hatchard, *Trans. Faraday Soc.* **1961**, *57*, 1894.

[16] S. Wu, M. Aonuma, Q. Zhang, S. Huang, T. Nakagawa, K. Kuwabara, C. Adachi, *J. Mater. Chem. C* **2014**, *2*, 421–424.

[17] Q. Zhang, J. Li, K. Shizu, S. Huang, S. Hirata, H. Miyazaki, C. Adachi, *J. Am. Chem. Soc.* **2012**, *134*, 14706–14709.

[18] A. S. Romanov, L. Yang, S. T. E. Jones, D. Di, O. J. Morley, B. H. Drummond, A. P. M. Reponen, M. Linnolahti, D. Credgington, M. Bochmann, *Chem. Mater.* **2019**, *31*, 3613–3623.

[19] R. Czerwieniec, J. Yu, H. Yersin, *Inorg. Chem.* **2011**, *50*, 8293–8301.

[20] J. Eng, T. J. Penfold, *Commun. Chem.* **2021**, *4*, 91.

[21] P. K. Samanta, D. Kim, V. Coropceanu, J.-L. Brédas, *J. Am. Chem. Soc.* **2017**, *139*, 4042–4051.

[22] B. T. Lim, S. Okajima, A. K. Chandra, E. C. Lim, *Chem. Phys. Lett.* **1981**, *79*, 22–27.

[23] C. M. Marian, *J. Phys. Chem. C* **2016**, *120*, 3715–3721.

[24] J. Gibson, A. P. Monkman, T. J. Penfold, *ChemPhysChem* **2016**, *17*, 2956–2961.

[25] M. K. Etherington, J. Gibson, H. F. Higginbotham, T. J. Penfold, A. P. Monkman, *Nat. Commun.* **2016**, *7*, 13680.

[26] P. L. Dos Santos, F. B. Dias, A. P. Monkman, *J. Phys. Chem. C* **2016**, *120*, 18259–18267.

[27] F. B. Dias, J. Santos, D. R. Graves, P. Data, R. S. Nobuyasu, M. A. Fox, A. S. Batsanov, T. Palmeira, M. N. Berberan-Santos, M. R. Bryce, A. P. Monkman, *Adv. Sci.* **2016**, *3*, 1600080.

[28] R. Hojo, D. M. Mayder, Z. M. Hudson, *J. Mater. Chem. C* **2021**, *9*, 14342–14350.

[29] H. Noda, X.-K. Chen, H. Nakanotani, T. Hosokai, M. Miyajima, N. Notsuka, Y. Kashima, J.-L. Brédas, C. Adachi, *Nat. Mater.* **2019**, *18*, 1084–1090.

[30] S. Montanaro, P. Pander, J.-R. Mistry, M. R. J. Elsegood, S. J. Teat, A. D. Bond, I. A. Wright, D. G. Congrave, M. K. Etherington, *J. Mater. Chem. C* **2022**, *10*, 6306–6313.

[31] P. L. dos Santos, J. S. Ward, M. R. Bryce, A. P. Monkman, *J. Phys. Chem. Lett.* **2016**, *7*, 3341–3346.

[32] Q. Zhang, D. Tsang, H. Kuwabara, Y. Hatae, B. Li, T. Takahashi, S. Y. Lee, T. Yasuda, C. Adachi, *Adv. Mater.* **2015**, *27*, 2096–2100.

[33] Q. Zhang, B. Li, S. Huang, H. Nomura, H. Tanaka, C. Adachi, *Nat. Photonics* **2014**, *8*, 326–332.

[34] H. Wang, L. Xie, Q. Peng, L. Meng, Y. Wang, Y. Yi, P. Wang, *Adv. Mater.* **2014**, *26*, 5198–5204.

[35] S. Y. Lee, C. Adachi, T. Yasuda, *Adv. Mater.* **2016**, *28*, 4626–4631.

[36] R. S. Nobuyasu, Z. Ren, G. C. Griffiths, A. S. Batsanov, P. Data, S. Yan, A. P. Monkman, M. R. Bryce, F. B. Dias, *Adv. Opt. Mater.* **2016**, *4*, 597–607.

[37] F. B. Dias, K. N. Bourdakos, V. Jankus, K. C. Moss, K. T. Kamtekar, V. Bhalla, J. Santos, M. R. Bryce, A. P. Monkman, *Adv. Mater.* **2013**, *25*, 3707–3714.

[38] P. L. dos Santos, J. S. Ward, D. G. Congrave, A. S. Batsanov, J. Eng, J. E. Stacey, T. J. Penfold, A. P. Monkman, M. R. Bryce, *Adv. Sci.* **2018**, *5*, 1700989.

[39] C. Fan, C. Duan, Y. Wei, D. Ding, H. Xu, W. Huang, *Chem. Mater.* **2015**, *27*, 5131–5140.

[40] R. Weh, A. de Klerk, *Energy Fuels* **2017**, *31*, 6607–6614.

[41] A. Salehi, X. Fu, D. Shin, F. So, *Adv. Funct. Mater.* **2019**, *29*, 1808803.

[42] J. M. Ha, S. H. Hur, A. Pathak, J.-E. Jeong, H. Y. Woo, *NPG Asia Mater.* **2021**, *13*, 53.

[43] T.-T. Bui, F. Goubard, M. Ibrahim-Ouali, D. Gigmes, F. Dumur, *Beilstein J. Org. Chem.* **2018**, *14*, 282–308.

[44] C. Qu, G. Xia, Y. Xu, Y. Zhu, J. Liang, H. Zhang, J. Wang, Z. Zhang, Y. Wang, *J. Mater. Chem. C* **2020**, *8*, 3846–3854.

[45] V. M. Hertz, J. G. Massoth, M. Bolte, H.-W. Lerner, M. Wagner, *Chem. Eur. J.* **2016**, *22*, 13181–13188.

[46] H. Zhao, F. P. Gabbaï, *Organometallics* **2012**, *31*, 2327–2335.

[47] Z. Yang, Z. Mao, Z. Xie, Y. Zhang, S. Liu, J. Zhao, J. Xu, Z. Chi, M. P. Aldred, *Chem. Soc. Rev.* **2017**, *46*, 915–1016.

[48] T. Hampel, S. Ruppenthal, D. Sälinger, R. Brückner, *Chem. Eur. J.* **2012**, *18*, 3136–3140.

[49] Deposition numbers 2169622 (for **3**), 2169623 (for **4**), 2169624 (for **7**), 2169625 (for **CZ-Dipp-SO2B**), 2169626 (for **PXZ-Dipp-SO2B**) and 2169627 (for **PXZ-Dipp-SO2B·CHCl3**) contain the supplementary crystallographic data for this paper. These data are provided free of charge by the joint Cambridge Crystallographic Data Centre and Fachinformationszentrum Karlsruhe Access Structures service.

[50] T. Jin, L. Kunze, S. Breimaier, M. Bolte, H.-W. Lerner, F. Jäkle, R. F. Winter, M. Braun, J.-M. Mewes, M. Wagner, *J. Am. Chem. Soc.* **2022**, *144*, 13704–13716.

[51] S. Kirschner, J.-M. Mewes, M. Bolte, H.-W. Lerner, A. Dreuw, M. Wagner, *Chem. Eur. J.* **2017**, *23*, 5104–5116.
[52] L. Giordano, V. V. Shvadchak, J. A. Fauerbach, E. A. Jares-Erijman, T. M. Jovin, *J. Phys. Chem. Lett.* **2012**, *3*, 1011–1016.
[53] M. Morimoto, Y. Takagi, K. Hioki, T. Nagasaka, H. Sotome, S. Ito, H. Miyasaka, M. Irie, *Dyes Pigm.* **2018**, *153*, 144–149.
[54] Y. Niko, S. Kawauchi, G. I. Konishi, *Chem. Eur. J.* **2013**, *19*, 9760–9765.
[55] H. Liu, X. Xu, H. Peng, X. Chang, X. Fu, Q. Li, S. Yin, G. J. Blanchard, Y. Fang, *Phys. Chem. Chem. Phys.* **2016**, *18*, 25210–25220.
[56] M. Okazaki, Y. Takeda, P. Data, P. Pander, H. Higginbotham, A. P. Monkman, S. Minakata, *Chem. Sci.* **2017**, *8*, 2677–2686.
[57] K. Stavrou, L. G. Franca, A. P. Monkman, *ACS Appl. Electron. Mater.* **2020**, *2*, 2868–2881.
[58] S. J. Strickler, R. A. Berg, *J. Chem. Phys.* **1962**, *37*, 814–822.
[59] G. Xia, C. Qu, Y. Zhu, J. Ye, K. Ye, Z. Zhang, Y. Wang, *Angew. Chem. Int. Ed.* **2021**, *60*, 9598–9603; *Angew. Chem.* **2021**, *133*, 9684–9689.
[60] H. Yersin, L. Mataranga-Popa, R. Czerwieniec, Y. Dovbii, *Chem. Mater.* **2019**, *31*, 6110–6116.
[61] L. G. Franca, Y. Long, C. Li, A. Danos, A. Monkman, *J. Phys. Chem. Lett.* **2021**, *12*, 1490–1500.
[62] J. S. Ward, R. S. Nobuyasu, A. S. Batsanov, P. Data, A. P. Monkman, F. B. Dias, M. R. Bryce, *Chem. Commun.* **2016**, *52*, 2612–2615.
[63] X. Zheng, R. Huang, C. Zhong, G. Xie, W. Ning, M. Huang, F. Ni, F. B. Dias, C. Yang, *Adv. Sci.* **2020**, *7*, 1902087.
[64] P. Pander, A. V. Zaytsev, A. Sil, J. A. G. Williams, P.-H. Lanoe, V. N. Kozhevnikov, F. B. Dias, *J. Mater. Chem. C* **2021**, *9*, 10276–10287.
[65] H. Yersin, A. F. Rausch, R. Czerwieniec, T. Hofbeck, T. Fischer, *Coord. Chem. Rev.* **2011**, *255*, 2622–2652.
[66] K. Sato, K. Shizu, K. Yoshimura, A. Kawada, H. Miyazaki, C. Adachi, *Phys. Rev. Lett.* **2013**, *110*, 247401.
[67] M. Chapran, P. Pander, M. Vasylieva, G. Wiosna-Salyga, J. Ulanski, F. B. Dias, P. Data, *ACS Appl. Mater. Interfaces* **2019**, *11*, 13460–13471.
[68] M. Sarma, K.-T. Wong, *ACS Appl. Mater. Interfaces* **2018**, *10*, 19279–19304.
[69] P. Pander, R. Daniels, A. V. Zaytsev, A. Horn, A. Sil, T. J. Penfold, J. A. G. Williams, V. N. Kozhevnikov, F. B. Dias, *Chem. Sci.* **2021**, *12*, 6172–6180.
[70] T. Hofbeck, U. Monkowius, H. Yersin, *J. Am. Chem. Soc.* **2015**, *137*, 399–404.
[71] P. Pander, R. Motyka, P. Zassowski, M. K. Etherington, D. Varsano, T. J. da Silva, M. J. Caldas, P. Data, A. P. Monkman, *J. Phys. Chem. C* **2018**, *122*, 23934–23942.

Manuscript received: November 28, 2022
Accepted manuscript online: January 9, 2023
Version of record online: January 24, 2023